SCIENCE CHINA
Chemistry

•ARTICLES•
SPECIAL ISSUE: 2023 Emerging Investigator Issue

December 2023 Vol.66 No.12: 3628–3635
https://doi.org/10.1007/s11426-023-1870-1

Transient spectral and dynamic properties of magic-size Cd_3P_2 nanoclusters in the limit of strong confinement

Yuan Liu[1,2], Yuxuan Li[2,3], Yupeng Yang[2,3], Jingyi Zhu[2*] & Kaifeng Wu[1,2,3*]

[1]*Department of Chemical Physics, University of Science and Technology of China, Hefei 230026, China;*
[2]*State Key Laboratory of Molecular Reaction Dynamics, Dalian Institute of Chemical Physics, Chinese Academy of Sciences, Dalian 116023, China;*
[3]*University of Chinese Academy of Sciences, Beijing 100049, China*

Received August 22, 2023; accepted November 4, 2023; published online November 14, 2023

Both semiconductor nanocrystals and organic molecules are important photofunctional materials for an array of applications. It is interesting to examine the intermediate regime between these two families, which can be interpreted as the strong-confinement limit of the nanocrystals or alternatively as the large-size limit of molecules. Here, we choose Cd_3P_2 magic-size clusters (MSCs) as a unique platform and apply time-resolved spectroscopy to investigate their spectral and dynamic properties. We find that these small clusters display molecular-like vibronic progression on their absorption and emission spectra and a large Stokes shift, which leads to well-separated transient absorption bleach and stimulated emission signals distinct from typical nanocrystals. On the other hand, such small size MSCs can still accommodate biexciton states, and the strongly enhanced Coulombic interactions lead to very fast dephasing of the biexciton resonance as well as rapid biexciton Auger annihilation (1.5 ps). Further, temperature-dependent measurements provide evidence for the transformation of band-edge excitons to localized excitons, with the localization likely driven by the softened lattice in these small-size clusters. These collective results demonstrate that strongly-confined nanoclusters indeed bridge the gap between nanocrystals and molecules, and can be a unique library to search for exotic excited state properties.

time-resolved spectroscopy, magic-size clusters, quantum confinement, excited-state dynamics

Citation: Liu Y, Li Y, Yang Y, Zhu J, Wu K. Transient spectral and dynamic properties of magic-size Cd_3P_2 nanoclusters in the limit of strong confinement. *Sci China Chem*, 2023, 66: 3628–3635, https://doi.org/10.1007/s11426-023-1870-1

1 Introduction

Semiconductor nanocrystals (NCs) are nanometer-scale materials exhibiting a plethora of attractive optical and electronic properties due to their quantum confinement effect [1,2]. Enabled by these properties, NCs have broad applications ranging from solar-energy conversion and light-emitting devices to biomedical diagnosis and therapeutics [3–6]. The fundamental photophysics of primary quasi-particle excitations in these materials, such as carriers and excitons, have also been well established and connected to their optoelectronic properties [1,7,8]. For example, strong carrier–carrier or exciton–exciton interactions are a typical signature of quantum-confined NCs, resulting in rapid non-radiative multicarrier or multiexciton Auger recombination that has become a major hurdle to their many applications mentioned above [9]. On the other hand, with the exception of charge-separated or defect-dominated NCs [10] or NCs featuring soft lattices [11], electron–phonon coupling is usually weak in NCs due to their rigid inorganic lattices and fully delocalized electron wavefunctions [12]. This is in direct contrast to another class of important photofunctional materials, molecules, for which strong vibronic coupling and nonadiabatic dynamics are their common features.

*Corresponding authors (email: kwu@dicp.ac.cn; jingyizh@dicp.ac.cn)

Nanoclusters with sizes typically smaller than 2 nm represent intermediate materials between NCs and small molecules [13]. Unlike NCs that inevitably show heterogeneities in their size and/or shape in an ensemble, these clusters often possess atomically-precise structures strongly resembling molecules. Indeed, molecular-like discrete electronic levels and strong vibronic coupling have been identified for atomically-precise metal clusters [14,15]. Parallel to metal clusters, semiconductor clusters termed magic-size clusters (MSCs) have also been developed [16–18]. Many studies in the past decades have been devoted to studying the formation and evolution of MSCs in colloidal synthesis, such as to better understand and control the nucleation and growth of colloidal NCs [19–23]. By contrast, the spectral and dynamic properties of these MSCs remain largely underexplored. A recent study found a large temperature-dependent band gap shift in $(CdSe)_{13}$ MSCs [24], revealing a strong interaction between excitons and phonons in these materials.

Here, we present a comprehensive spectroscopic study on II–V group Cd_3P_2 MSCs. The bulk bandgap of Cd_3P_2 is 0.55 eV, and therefore the Cd_3P_2 MSCs with an optical gap at 450 nm (2.755 eV) is situated in the extremely strong confinement regime. Meanwhile, the visible optical gap allows us to study their transient spectra and dynamic properties using a suite of steady-state and time-resolved spectroscopic tools, under varying pump-fluence or temperature conditions. Unlike previous studies on metal clusters or doped MSCs focusing on the size-dependent evolution of electronic properties [25,26], here, we find that Cd_3P_2 MSCs simultaneously accommodate both NC and molecular behaviors. We therefore provide evidence that strongly-confined MSCs represent an intermediate state of matter between NCs and molecules.

2 Results and discussion

2.1 Steady-state and transient spectra

We synthesized Cd_3P_2 MSCs using a thermodynamically driven method reported in the literature [27], with details provided in the Supporting Information (SI). The transmission electron microscopy (TEM) image shows that these MSCs have a diameter of ~2 nm (Figure S1), but this is just an upper limit as we cannot exclude the aggregation of these MSCs upon the deposition onto substrates and irradiated by electron beams [28–30]. Further structural, elemental and chemical characterizations of these MSCs can be found in ref. [27]. The bulk Bohr diameter of Cd_3P_2 is ~40 nm [31–34], and therefore, these MSCs are indeed situated in the limit of very strong quantum confinement, as their size is much smaller than the natural length scale of the excitons in Cd_3P_2.

The room-temperature absorption and photoluminescence (PL) spectra of as-synthesized Cd_3P_2 MSCs dispersed in hexane are presented in Figure 1a. The band edge absorption peak located at ~450 nm (~2.755 eV) is fairly narrow, with a full width at half maximum (FWHM) of ~15 nm (~0.1 eV), and is almost completely isolated from the higher-energy absorption features. Such a clean isolation of the lowest absorption peak has been rarely observed in the absorption spectra of typical colloidal NCs, but is typical for small molecules. The room-temperature PL spectrum also shows a sharp peak centered at ~458 nm (~2.707 eV), with a FWHM nearly identical to that of the absorption peak. The large Stokes shift (~47 meV) of the band-edge emission indicates that the nuclei strongly are re-organized in the photoexcited state. In addition, the absorption and PL peaks is symmetrically broadened towards short and long wavelengths, respectively. Such a mirror symmetry is reminiscent of the vibronic progression observed for molecules.

We further carried out femtosecond transient absorption (TA) measurements of Cd_3P_2 MSCs at room temperature to reveal their excited-state spectral properties; see supporting information for experimental details. Figure 1b displays a typical TA spectrum monitored at a pump-probe delay time of 0.4 ps following a near-resonance excitation (440 nm) with a pump fluence of ~11 μJ cm^{-2}. Detailed spectral evolution will be discussed below; here we focus on the early-time TA spectral shape. The TA spectrum consists of strong bleach and red-side and blue-side photoinduced absorption (PIA) features encompassing the bleach feature. Compared with the ground-state spectra, we find that the bleach is red-shifted from the ground-state absorption peak and can be decomposed into an exciton bleach (XB) feature and a stimulated emission (SE) feature. This is a clear distinction from NCs for which a SE feature has been rarely observed in the single-exciton regime due to (1) the similar energy of single-exciton absorption and emission, and (2) the small energy difference between ground-to-exciton and exciton-to-biexciton transitions [9]. Thus, the simultaneous presence of XB and SE features observed in Cd_3P_2 MSCs strongly resembles a molecular behavior.

For NCs, the PIA feature on the red-side of XB is typically very weak and is attributed to the exciton-to-biexciton transition being slightly red-shifted from the ground-to-exciton transition, with the shift corresponding to the biexciton binding energy [9] (see Figure S4 for representative data for a sample of Cd_3P_2 NCs). On the other hand, the blue-side PIA of NCs is typically associated with the shift of higher-energy exciton features. Herein, however, the absence of high-energy excitons near the lowest exciton rules out this possibility. Therefore, both red- and blue-side PIAs are associated with the lowest exciton transition. A straightforward interpretation is a strong broadening of the excited-state absorption (ESA) in the presence of an exciton. Because this

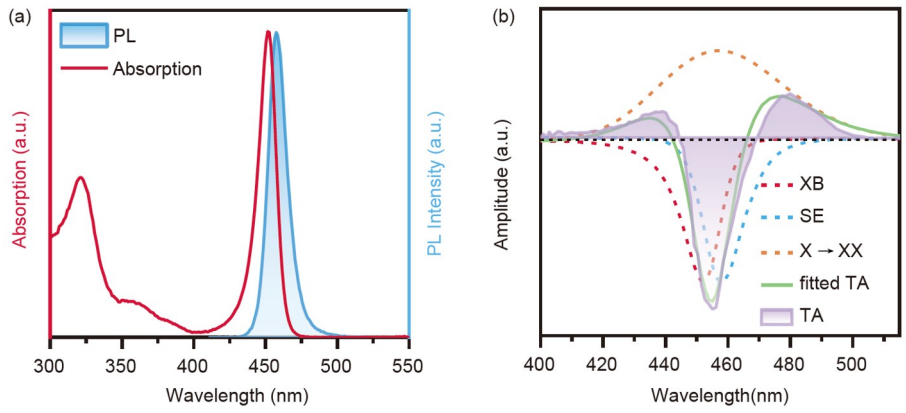

Figure 1 Steady-state and transient spectra of Cd_3P_2 MSCs. (a) UV-vis absorption (red solid line) and photoluminescence (PL; blue shaded curve) spectra of Cd_3P_2 MSCs dispersed in hexane at room temperature. The PL was collected with 350 nm excitation. (b) Transient absorption (TA) spectrum (purple shaded curve) of Cd_3P_2 MSCs monitored at a pump-probe delay time of 0.4 ps following 440 nm pump with a fluence of ~11 μJ cm^{-2}. The exciton bleach (XB), stimulated emission (SE) and exciton-to-biexciton (X→XX) absorption features obtained from spectral decomposition are also plotted. The fitted TA (green solid line) represents the sum of the three decomposed spectra, which strongly resembles the measured TA spectrum (purple shaded curve) (color online).

ESA is still centered around the exciton feature, we attribute it to the exciton-to-biexciton transition. To obtain the spectrum of this transition, we perform a spectral fit to the experimental TA spectrum. We represent this transition using a single Gaussian band, and we further scale the steady-state absorption and PL peaks to obtain their contributions to the XB and SE features, respectively, on the TA spectrum. By adding the spectra of these three species together, we can fit the experimental spectrum, with the scaling coefficients for the absorption and PL peaks and the width (FWHM) of the exciton-to-biexciton Gaussian band as fitting parameters. The fitting spectrum closely resembles the experimental one, although there are subtle features not being captured by this simple spectral decomposition. Through this fit, we find that the exciton-to-biexciton transition has a FWHM of 0.28 eV, corresponding to a dephasing time of ~5 fs. Such rapid dephasing indicates strong Coulombic scattering between excitons, which is induced by the extreme confinement in these Cd_3P_2 MSCs. Dephasing induced by exciton–exciton scattering was previously found for a variety of low-dimensional systems featuring strong Coulombic interactions, including epitaxial quantum wells [35,36], semiconducting carbon nanotubes [37,38] and more recently monolayer transition-metal dichalcogenides [39–41]. However, scattering-induced broadening in these materials was typically smaller than 10 meV even at their highest excitation densities. The much stronger broadening observed here can be attributed to the exceptionally high exciton densities accessible in our Cd_3P_2 MSCs. Assuming a spherical particle with a diameter of 2 nm (volume of 4.2×10^{-21} cm^3), putting two excitons into a particle would result in an exciton density of ~5×10^{20} cm^{-3}.

2.2 Exciton relaxation dynamics

TA measurements provide access to not only transient spectra but also ultrafast evolution of photoexcited states of Cd_3P_2 MSCs. Figure 2a presents the group-delay-corrected two-dimensional (2D) TA spectrum within 2 ns. We have briefly analyzed the above TA spectrum at 0.4 ps; here, we further investigate the full-spectral time evolution by globally fitting the data using a sequential kinetic model of relaxation (see supporting information for details). This model allows us to extract relevant kinetic time constants and associated species spectra. The simulated 2D spectrum is presented in Figure 2b, which is in quantitative agreement with the experimental spectrum in Figure 2a. The high quality of the global fit is also confirmed by the good match between experimental and simulated TA spectrum at indicated time or kinetic traces plotted at several representative wavelengths (Figure S2). The extracted species spectra and their corresponding dynamics are plotted in Figure 2c and 2d, respectively. We find that at least 4 species are required in the simulation to reproduce the experimental 2D spectrum. The first two species (S_1 and S_2) have in general a similar spectral shape, which has been assigned to a superposition of an XB feature, a SE feature and a broadened exciton-to-biexciton absorption feature. Based on this spectral shape and pump-intensity-dependent experiments as presented below, we assign S_2 to the single-excitons and S_1 to a mixed population of single-excitons and biexcitons, and the 1.5 ps lifetime of S_1 is related to biexciton Auger recombination (see below). The close similarity between the spectra of S_1 and S_2 suggests that the relative population of biexcitons compared with excitons is small at this pump fluence.

S_2 (*i.e.*, band-edge single-excitons) decays in 13 ps to form S_3 whose bleach feature is considerably weaker in the red regime than that of S_2, indicating that the SE feature is absent in S_3. In addition, the broad exciton-to-biexciton absorption is strongly suppressed for S_3. These results suggest that S_3 is no longer a band-edge exciton in Cd_3P_2 MSCs and is tenta-

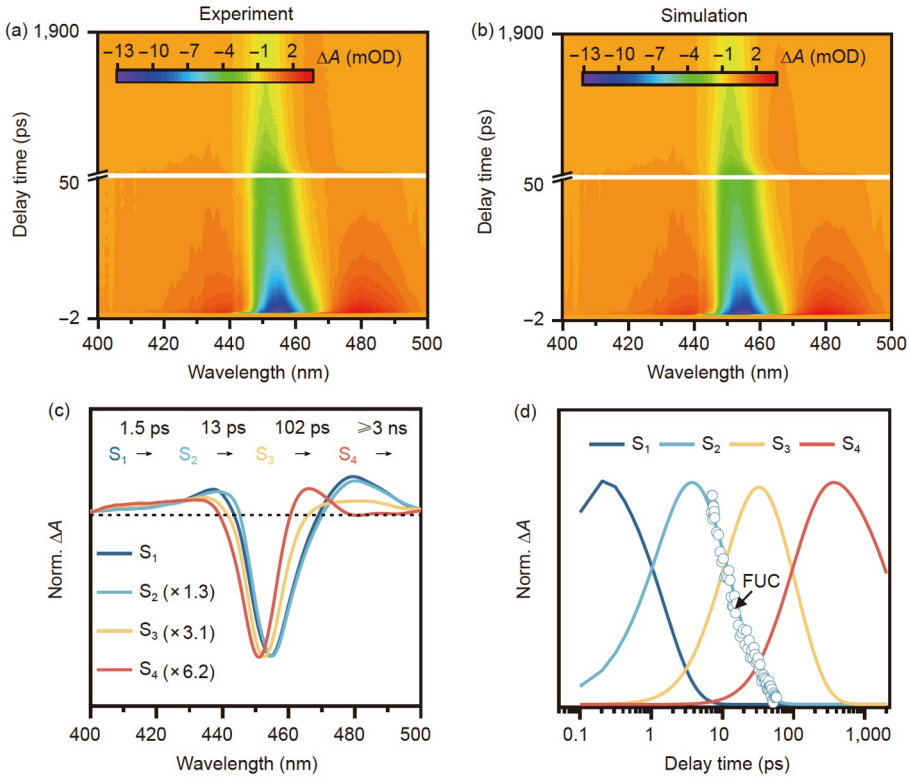

Figure 2 Global analysis of the TA spectra of Cd_3P_2 MSCs. (a, b) Experimental (a) and simulated (b) 2D TA spectra of Cd_3P_2 MSCs following excitation at 440 nm of 11 μJ cm^{-2} at room temperature. The simulation was based on a sequential decay kinetic model. (c, d) Normalized transient species spectra (c) and their corresponding dynamics (d) obtained from global fit. There are four species S_1, S_2, S_3 and S_4 with corresponding lifetimes of 1.5 ps,13 ps,102 ps and >3 ns, respectively. Note that the spectra in (c) are scaled by appropriate factors in order to better compare their spectral shapes. In (d), the femtosecond fluorescence upconversion (FUC) kinetics of the band-edge emission at 460 nm is also plotted for comparison (open circles), which is consistent with the decay of S_2 (color online).

tively assigned to a localized exciton species. Note here we define the band-edge exciton as the one that is fully delocalized in the whole cluster with the exciton energy matching the optical gap of this material, whereas the localized exciton is a species that is located at a site either inside the cluster or on the surface, and its energy is strongly renormalized due to a large reorganization energy associated with the change in the nuclear coordinates. This is further supported by our time-resolved PL measurements of the Cd_3P_2 MSCs conducted using a femtosecond fluorescence upconversion (FUC) setup with a sub-ps resolution (see supporting information for details). The FUC kinetics of the band-edge emission at 460 nm at room temperature decays in 15.8 ps, which is in very good agreement with the fitted TA decay of S_2 (Figure 2d). The exact mechanism responsible for the transformation of a band-edge exciton to a localized exciton remains unclear, but we suspect that this could be triggered by lattice distortion in these small-size MSCs (see below). These localized excitons further decay in 102 ps to form S_4 whose spectrum consists of a blueshifted bleach and a red-side absorption. This derivative-like spectral shape suggests that S_4 is likely related to a charge-separated species with a carrier (either electron or hole) captured by surface traps [42]. This charge-separated state is long-lived, with a lifetime exceeding 3 ns.

2.3 Biexciton Auger recombination

Pump-power-dependent TA measurements were performed to further confirm the accommodation of biexcitons in the Cd_3P_2 MSCs and to observe their rapid Auger recombination. Figure 3a presents the TA spectra at ~0.4 ps following 440 nm excitation of varying pulse fluences. In the fluence range of 11 to 150 μJ cm^{-2}, the overall signal amplitudes increase with the fluences and then gradually approach saturation (Figure 3a and Figure S3). However, the saturation behavior is slightly different for the XB feature and the broad exciton-to-biexciton absorption feature (Figure S3). As revealed by comparing the TA spectra under 11 and 150 μJ cm^{-2} in Figure 3b, the intensity of the exciton-to-biexciton absorption relative to the XB is reduced at 150 μJ cm^{-2}, which is consistent with a higher occupancy of biexcitons at higher fluences.

To analyze the population dynamics of the photoexcited species, the whole TA signal in the observed spectral region is integrated, and the resultant time-dependent integral in-

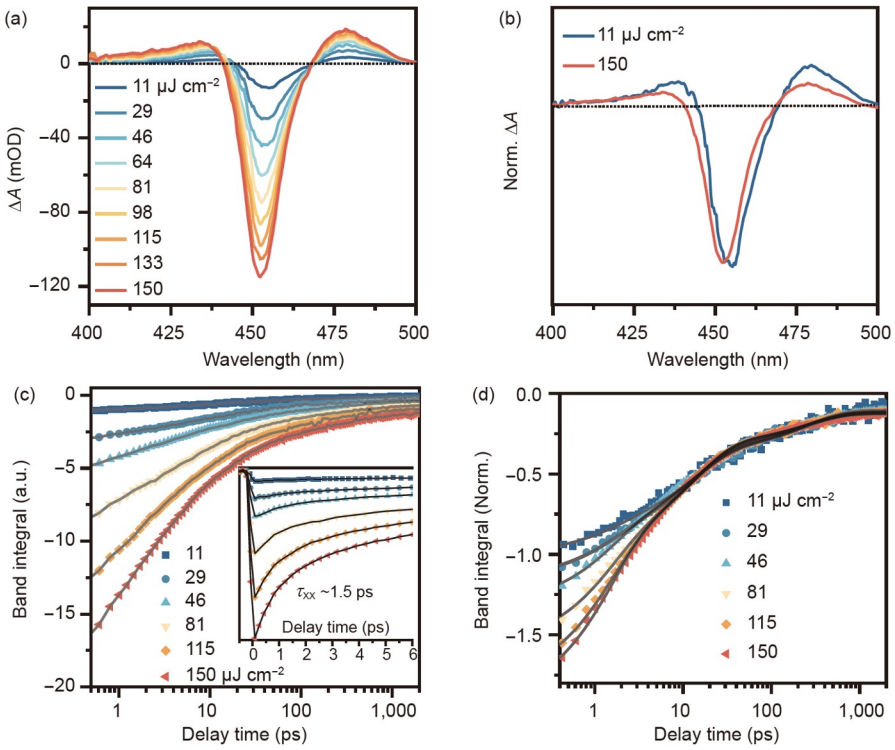

Figure 3 Pump-fluence-dependent TA measurements of Cd_3P_2 MSCs. (a) TA spectra at 0.4 ps following excitation at 440 nm of varying fluences from 11 to 151 μJ cm^{-2}. (b) Comparison between the TA spectra at 11 and 151 μJ cm^{-2} to reveal their distinct spectral shapes. (c) Time-dependent integrated TA signal intensities (400–510 nm) at varying pump fluences (colored symbols) and their global fits (black solid lines) ones. Inset is an enlarged view of the dynamics with the first 2 ps. (d) Replot of the fluence-dependent kinetic traces in (c) by normalizing them at their slow tails, which clearly reveals the rapid biexciton Auger recombination with a time constant of 1.5 ps (color online).

tensities at varying pump fluences are presented in Figure 3c. These kinetic traces can be globally fitted using the set of time constants described in Figure 2d, but the relative amplitude of the biexcitons increases with the pump fluence (inset of Figure 3c). To better visualize the biexciton components, in Figure 3d, we also plot the fluence-dependent kinetic traces by normalizing them at their slow tails. The exceptionally rapid biexciton Auger recombination (τ_{XX} = 1.5 ps) is consistent with the extreme confinement of excitons in the Cd_3P_2 MSCs strongly enhancing Coulombic interactions. In a previous study of Cd_3P_2 NCs of 2.6 nm diameter, τ_{XX} was measured to be 3.6 ps [34]. Using a simple volume-scaling law established for τ_{XX}, we can estimate a diameter of 1.9 nm for the Cd_3P_2 MSCs, which is roughly consistent with the TEM image in Figure S1. However, we note that this is only qualitative estimation, as it remains unclear whether the typical scaling laws established in NCs can be extrapolated to the extreme confinement regime of the MSCs [43].

2.4 Temperature-dependent exciton localization and trapping

To obtain further insights into the exciton localization and trapping dynamics following biexciton Auger recombination, we performed temperature-dependent steady-state and time-resolved PL measurements of Cd_3P_2 MSCs. The MSCs solution filled in an 1 mm cuvette were placed in a cryostat to control the sample temperature. Figure 4a presents the steady-state PL spectra at varying temperatures from 115 K to 310 K. Decreasing temperature results in the blueshift, narrowing and enhancement of the band-edge exciton emission. Temperature-dependent steady-state absorption and PL spectra display simultaneous blueshift and narrowing behaviors, which are typical for semiconductor materials, and the latter can be analyzed using the Varshni model (Figure S5). Thus, in spite of their extremely small sizes, MSCs still inherit some intrinsic band properties of their bulk parents. In addition to the band-edge emission, decreasing temperature results in the emergence and increasing of a broadband emission in the range of ~500–800 nm (FWHM ~0.5 eV). As a result, while the Cd_3P_2 MSCs show a pure blue emission at room temperature, they emit white light at 115 K. Such a white-light emission was previously observed in CdSe MSCs and small-size CdSe and CdS NCs [44–46]. The room-temperature PL quantum yield (QY) of our Cd_3P_2 MSCs was estimated to be ~7% using an integrating sphere method, on the basis of which the PL QY of the whole emission spectrum reaches ~41% at 115 K.

The reasons for the temperature dependence of the PL

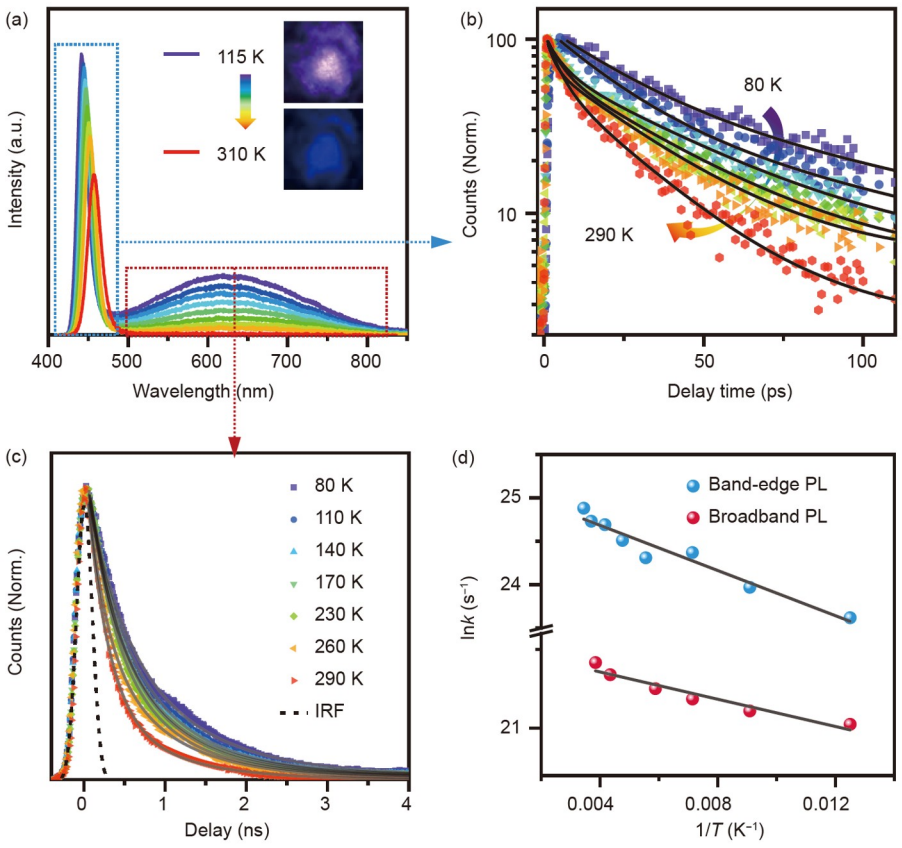

Figure 4 Temperature-dependent PL measurements of Cd_3P_2 MSCs. (a) Steady-state PL spectra at varying temperatures from 115 K to 310 K under 375 nm excitation. Insets show the optical images of the sample film at 115 K (white color) and 310 K (blue color). (b) FUC kinetics of the band-edge exciton PL measured at varying temperatures from 290 K to 80 K (colored symbols) and their exponential fits (solid lines). (c) TCSPC kinetics of the broadband PL of localized excitons measured at varying temperatures from 290 K to 80 K (colored symbols) and their exponential fits (solid lines). The bump on the 80 K TCSPC curve is an artifact. (d) Plots of ln(k), where k is the temperature-dependent decay rate, as a function of the inverse of temperature (1/T) for band-edge exciton PL (blue solid circle) and broadband PL (red solid circle) and their fits (solid lines). The activation energies are found to be 11.2 and 3.7 meV for the decay of the band-edge exciton PL and broadband PL, respectively (color online).

spectra of Cd_3P_2 MSCs can be uncovered by time-resolved PL measurements. As plotted in Figure 4b, the band-edge exciton PL dynamics measured by FUC shows a slower decay with decreasing temperature. At 290 K, the PL lifetime is only 15.8 ps, consistent with the 13 ps lifetime of S_2 revealed in TA measurements. Accounting for a PL QY of 7%, we estimate the room-temperature radiative lifetime of band-edge excitons to be ~226 ps. At 80 K, the band-edge PL lifetime is prolonged to 53.8 ps, which explains the enhancement of the band-edge PL at low temperatures. In Figure 4d, we present the temperature-dependent decay rates (k) of the band-edge PL using an Arrhenius-type plot, *i.e*, ln(k) as a function of the inverse of temperature (1/T). Fitting the data reveals an activation energy ($E_{a,1}$) of 11.2 meV for the decay of band-edge excitons into localized excitons. These localized excitons are responsible for the broadband emission observed in Figure 4a. We measured the decay dynamics of this broadband emission at varying temperatures using time-correlated single photon counting (TCSPC; see supporting information). At 290 K, the decay curve is mostly limited by the instrument response function of ~230 ps (Figure 4c), consistent with the 102 ps lifetime of S_3 revealed in TA measurements. With decreasing temperature, the decay is also gradually slowed down. By making an Arrhenius-type analysis similar to that of the band-edge PL (Figure 4d), we find an activation energy ($E_{a,2}$) of 3.7 meV for the decay of the broadband emission associated with localized excitons. On the basis of the estimated QY of 28% for the broadband emission at 115 K and the corresponding lifetime of 680 ps, the radiative lifetime of the localized excitons is estimated to be ~2.4 ns at 115 K.

2.5 Discussion

The experiments and analysis above allow us to obtain a complete picture of the excited-state dynamics in Cd_3P_2 MSCs, which is depicted in Figure 5. The ground state is promoted by the photoexcitation to the single-exciton or biexcitons states, depending upon the excitation power. The biexcitons are annihilated to single-excitons within 1.5 ps

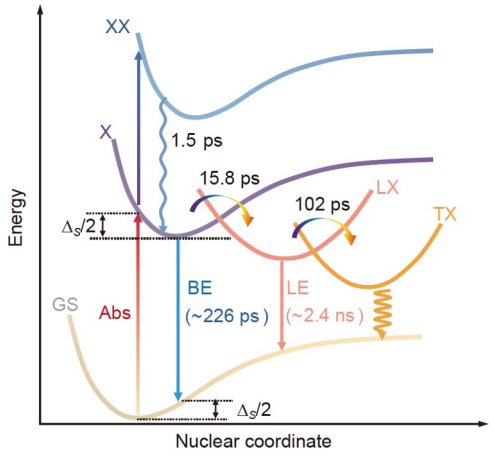

Figure 5 Summary of excited-state dynamics in Cd_3P_2 MSCs. The states are plotted in terms of their energies (ordinate) and nuclear coordinates (abscissa). GS stands for the ground state, and X and XX stand for single-exciton and biexciton states, respectively. LX is a localized exciton state, whereas TX is a trapped exciton. Straight arrows stand for optical transitions and wavy arrows are nonradiative transitions. BE and LE stand for band-edge emission and localized exciton emission, respectively. Relevant time constants are indicated (color online).

through the Auger recombination. The nuclei coordinates of the excitonic states are more considerably displaced than the ground states, resulting in a band-edge emission with a fairly large Stoke shift (~47 meV). The single-excitons are transformed to localized excitons within 15.8 ps at room temperature, with an activation barrier of ~11.2 meV. The localized excitons have drastically displaced nuclei coordinates compared with the ground state, thus giving rise to very broad emission (FWHM ~500 meV) containing a large number of vibronic progressions. These localized excitons are further captured by trap states within 102 ps at room temperature, with an activation barrier of ~3.7 meV, and finally the trapped excitons decay back to ground states mostly through the nonradiative recombination.

The localized excitons with the broadband emission and slow radiative decay are reminiscent of self-trapped excitons (STEs) observed in a wide variety of metal halide semiconductors [47–53]. The softness of these materials leads to a strong distortion of their lattices upon the photoexcitation. In principle, II–V semiconductors should have rigid crystal lattices different from these soft materials. However, when the sizes of NCs are reduced to those of MSCs, the crystal structure could become highly dynamic, as has been predicted by theory [54–56]. For example, it has been observed that the scanning TEM images of very small CdSe NCs showed highly-disordered lattices, indicating the dynamic disorder induced by electron beams [57]. Although electron beams and photons interact with materials in different fashions, the photoexcitation could in principle also cause the strong lattice distortion in these MSCs. Previous studies have also invoked such a mechanism to explain the broad-band emission observed in CdSe MSCs [45,58,59]. Nevertheless, we cannot exclude the possibility that localization sites are situated on the surfaces of MSC, as in these small MSCs the surfaces could also become highly dynamic upon photoexcitation to form exciton localization sites [49,58–62]. We note that, in spite of the strong electron–phonon interaction in these MSCs, we did not detect coherent phonon beats on the TA kinetic traces (*e.g.*, Figure 3c). It is likely that the highly dynamic lattice results in broadly-distributed and/or overdamped phonon modes. As to the final trap states (S_4 revealed in TA), we tentatively associate them with charge-separated species induced by surface trapping. The major evidence is that they have a derivative-like TA spectrum (Figure 2c) that has been frequently observed in previous studies of charge transfer from photoexcited NCs [42]. Specifically, charge separation sets up an interfacial electric field around a NC, and this field shifts the absorption spectrum of an exciton transition through the d.c. Stark effect [63].

3 Conclusions

In conclusion, we have systematically investigated the optical transition and associated excited state relaxation dynamics in colloidal Cd_3P_2 MSCs by using a suite of time-resolved spectroscopy tools. We find that due to the extremely strong quantum confinement effect, these MSCs simultaneously display molecular and NC like properties of optical responses. On one hand, the absorption and emission spectra show vibronic-like progression, with a large Stokes shift of ~47 meV. This leads to simultaneous presence of absorption bleach and stimulated emission on their TA spectra, which is distinct from typical NCs or quantum dots (QDs). On the other hand, similar to QDs, such very small size MSCs still can accommodate biexciton states. Importantly, the strongly enhanced Coulombic interactions lead to very fast dephasing of the biexciton resonance (~5 fs) as well as the rapid biexciton Auger annihilation (1.5 ps). Thus, these MSCs provide an ideal model for studying many-body interactions in the strong limit of three-dimensional confinement beyond strongly-confined QDs. Temperature-dependent time-resolved PL studies allow us to further track the evolution of band-edge single-excitons ensuing biexciton annihilation and to identify the evidence for the lattice-induced exciton localization. Such localized excitons give rise to a broadband emission (FWHM ~500 meV) reminiscent of self-trapped excitons observed in recent metal-halide materials featuring soft lattices. Thus, the extreme confinement in MSCs seems also to have important consequence for lattice dynamics and could significantly soften the originally rigid lattices of their parent materials. These rich photophysical properties revealed in MSCs can stimulate future searching

of many exotic spectral and dynamic properties in the extremely strong confinement regime.

Acknowledgements K.W. acknowledges financial support from the Chinese Academy of Sciences (YSBR-007), the National Natural Science Foundation of China (22173098, 21975253), the Fundamental Research Funds for the Central Universities (20720220009) and the New Cornerstone Science Foundation through the XPLORER PRIZE.

Conflict of interest The authors declare no conflict of interest.

Supporting information The supporting information is available online at chem.scichina.com and link.springer.com/journal/11426. The supporting materials are published as submitted, without typesetting or editing. The responsibility for scientific accuracy and content remains entirely with the authors.

1 Efros AL, Rosen M. *Annu Rev Mater Sci*, 2000, 30: 475–521
2 Alivisatos AP. *Science*, 1996, 271: 933–937
3 Shirasaki Y, Supran GJ, Bawendi MG, Bulović V. *Nat Photon*, 2013, 7: 13–23
4 Kramer IJ, Sargent EH. *Chem Rev*, 2014, 114: 863–882
5 de Arquer FPG, Talapin DV, Klimov VI, Arakawa Y, Bayer M, Sargent EH. *Science*, 2021, 373: eaaz8541
6 Kagan CR, Lifshitz E, Sargent EH, Talapin DV. *Science*, 2016, 353: aac5523
7 Brus LE. *J Chem Phys*, 1983, 79: 5566–5571
8 Brus LE. *J Chem Phys*, 1984, 80: 4403–4409
9 Klimov VI. *Annu Rev Phys Chem*, 2007, 58: 635–673
10 Knowles KE, Hartstein KH, Kilburn TB, Marchioro A, Nelson HD, Whitham PJ, Gamelin DR. *Chem Rev*, 2016, 116: 10820–10851
11 Brennan MC, Herr JE, Nguyen-Beck TS, Zinna J, Draguta S, Rouvimov S, Parkhill J, Kuno M. *J Am Chem Soc*, 2017, 139: 12201–12208
12 Kelley AM. *J Phys Chem Lett*, 2010, 1: 1296–1300
13 Zhou M, Jin R. *Annu Rev Phys Chem*, 2021, 72: 121–142
14 Zhou M, Higaki T, Hu G, Sfeir MY, Chen Y, Jiang D, Jin R. *Science*, 2019, 364: 279–282
15 Kong J, Wu Y, Zhou M. *Chin J Chem Phys*, 2021, 34: 598–604
16 Herron N, Calabrese JC, Farneth WE, Wang Y. *Science*, 1993, 259: 1426–1428
17 Lee GSH, Craig DC, Ma I, Scudder ML, Bailey TD, Dance IG. *J Am Chem Soc*, 1988, 110: 4863–4864
18 Dance IG, Choy A, Scudder ML. *J Am Chem Soc*, 1984, 106: 6285–6295
19 Shen Q, Luan C, Rowell N, Zhang M, Wang K, Willis M, Chen X, Yu K. *Inorg Chem*, 2021, 60: 4243–4251
20 He L, Luan C, Rowell N, Zhang M, Chen X, Yu K. *Acc Chem Res*, 2021, 54: 776–786
21 Pun AB, Mule AS, Held JT, Norris DJ. *Nano Lett*, 2021, 21: 7651–7658
22 Hens Z, De Roo J. *J Am Chem Soc*, 2020, 142: 15627–15637
23 Bootharaju MS, Baek W, Lee S, Chang H, Kim J, Hyeon T. *Small*, 2021, 17: 2002067
24 Muckel F, Lorenz S, Yang J, Nugraha TA, Scalise E, Hyeon T, Wippermann S, Bacher G. *Nat Commun*, 2020, 11: 4127
25 Zhou M, Zeng C, Chen Y, Zhao S, Sfeir MY, Zhu M, Jin R. *Nat Commun*, 2016, 7: 13240
26 Kwon Y, Oh J, Lee E, Lee SH, Agnes A, Bang G, Kim J, Kim D, Kim S. *Nat Commun*, 2020, 11: 3127
27 Wang R, Ratcliffe CI, Wu X, Voznyy O, Tao Y, Yu K. *J Phys Chem C*, 2009, 113: 17979–17982
28 Palencia C, Yu K, Boldt K. *ACS Nano*, 2020, 14: 1227–1235
29 Vossmeyer T, Reck G, Katsikas L, Haupt ETK, Schulz B, Weller H. *Science*, 1995, 267: 1476–1479
30 Dong A, Chen J, Vora PM, Kikkawa JM, Murray CB. *Nature*, 2010, 466: 474–477
31 Sierański K, Szatkowski J, Misiewicz J. *Phys Rev B*, 1994, 50: 7331–7337
32 Lin-Chung PJ. *Phys Stat Sol (b)*, 1971, 47: 33–39
33 Andrzejewski J, Misiewicz J. *Phys Stat Sol (b)*, 2001, 227: 515–540
34 Wu K, Liu Z, Zhu H, Lian T. *J Phys Chem A*, 2013, 117: 6362–6372
35 Honold A, Schultheis L, Kuhl J, Tu CW. *Phys Rev B*, 1989, 40: 6442–6445
36 Wang H, Ferrio K, Steel DG, Hu YZ, Binder R, Koch SW. *Phys Rev Lett*, 1993, 71: 1261–1264
37 Nguyen DT, Voisin C, Roussignol P, Roquelet C, Lauret JS, Cassabois G. *Phys Rev Lett*, 2011, 107: 127401
38 Koyama T, Yoshimitsu S, Miyata Y, Shinohara H, Kishida H, Nakamura A. *J Phys Chem C*, 2013, 117: 20289–20299
39 Boule C, Vaclavkova D, Bartos M, Nogajewski K, Zdražil L, Taniguchi T, Watanabe K, Potemski M, Kasprzak J. *Phys Rev Mater*, 2020, 4: 034001
40 Katsch F, Selig M, Knorr A. *Phys Rev Lett*, 2020, 124: 257402
41 Moody G, Dass CK, Hao K, Chen CH, Li LJ, Singh A, Tran K, Clark G, Xu X, Berghäuser G, Malic E, Knorr A, Li X. *Nat Commun*, 2015, 6: 8315
42 Zhu H, Yang Y, Wu K, Lian T. *Annu Rev Phys Chem*, 2016, 67: 259–281
43 Chen Z, Beimborn II JC, Kirkwood N, Russo SP, Weber JM, Mulvaney P. *J Phys Chem C*, 2023, 127: 8657–8669
44 Bowers MJ, McBride JR, Rosenthal SJ. *J Am Chem Soc*, 2005, 127: 15378–15379
45 Beecher AN, Yang X, Palmer JH, LaGrassa AL, Juhas P, Billinge SJL, Owen JS. *J Am Chem Soc*, 2014, 136: 10645–10653
46 Jethi L, Mack TG, Kambhampati P. *J Phys Chem C*, 2017, 121: 26102–26107
47 Yang B, Han K. *J Phys Chem Lett*, 2021, 12: 8256–8262
48 Smith MD, Karunadasa HI. *Acc Chem Res*, 2018, 51: 619–627
49 Song K, Williams RT. *Self-trapped Excitons*. Berlin: Springer, 2013
50 Jiang F, Wu Z, Lu M, Gao Y, Li X, Bai X, Ji Y, Zhang Y. *Adv Mater*, 2023, 35: 2211088
51 Ueta M, Kanzaki H, Kobayashi K, Toyozawa Y, Hanamura E, Ueta M, Kanzaki, H, Kobayashi K, Toyozawa Y, Hanamura E. Theory of Excitons in Phonon Fields. In: *Excitonic Processes in Solids*, Berlin: Springer, 1986, 203–284
52 Li M, Xia Z. *Chem Soc Rev*, 2021, 50: 2626–2662
53 Iwanaga M, Azuma J, Shirai M, Tanaka K, Hayashi T. *Phys Rev B*, 2002, 65: 214306
54 Franceschetti A, Pantelides ST. *Phys Rev B*, 2003, 68: 033313
55 Degoli E, Cantele G, Luppi E, Magri R, Ninno D, Bisi O, Ossicini S. *Phys Rev B*, 2004, 69: 155411
56 Franceschetti A. *Phys Rev B*, 2008, 78: 075418
57 Pennycook TJ, McBride JR, Rosenthal SJ, Pennycook SJ, Pantelides ST. *Nano Lett*, 2012, 12: 3038–3042
58 Bawendi MG, Carroll PJ, Wilson WL, Brus LE. *J Chem Phys*, 1992, 96: 946–954
59 Landes CF, Braun M, El-Sayed MA. *J Phys Chem B*, 2001, 105: 10554–10558
60 Vörös M, Galli G, Zimanyi GT. *ACS Nano*, 2015, 9: 6882–6890
61 Allan G, Delerue C, Lannoo M. *Phys Rev Lett*, 1996, 76: 2961–2964
62 Puzder A, Williamson AJ, Gygi F, Galli G. *Phys Rev Lett*, 2004, 92: 217401
63 Wu K, Zhu H, Liu Z, Rodríguez-Córdoba W, Lian T. *J Am Chem Soc*, 2012, 134: 10337–10340